An Integrated Cross-Layer Study of Wireless CDMA Sensor Networks

Swades De, *Student Member, IEEE*, Chunming Qiao, *Member, IEEE*, Dimitris A. Pados, *Member, IEEE*, Mainak Chatterjee, and Sumesh J. Philip

***Abstract*—In this paper, we characterize analytically the multiaccess interference in wireless code-division multiple-access sensor networks with uniformly random distributed nodes and study the tradeoff between interference and connectivity. To provide a guideline for improving system behavior, three competitive deterministic topologies are evaluated along with the random topology in terms of link-level and network-level (routing) performance. The impact of signature code length and receiver design on the network performance for different topologies is also studied.**

***Index Terms*—Ad hoc networks, code-division-multiple-access (CDMA), interference suppression, network connectivity, network topology, spreading signatures, throughput, wireless sensor networks.**

I. Introduction and Motivation

WE CONSIDER a wireless sensor network which may contain thousands of tiny low-cost sensors scattered over a region of interest [1], [2]. The sensors (also called nodes) are battery operated (i.e., energy constrained), have limited memory and processing power, and form a randomly connected ad hoc network. The nodes are mostly stationary and their location information may be obtained via global positioning system (GPS) or other means [3]–[6] to assist efficient information processing (e.g., data aggregation) and distributed routing.

Given that the sensors have limited energy, buffer space, and other resources, contention-based protocols-based, for example, on the 802.11 direct-sequence spread-spectrum (DS-SS) technique may not be a suitable option. Here, as an alternative, we suggest code-division multiplexing, where distinct codes (signatures) can be allocated to different nodes with possible code reuse between spatially separated nodes as in cellular CDMA systems. The use of multiple properly designed codes will reduce the channel access conflict at the expense of multiaccess interference (MAI), which is absent in 802.11 DS-SS systems.

Manuscript received October 1, 2003; revised March 15, 2004. This work was supported in part by the National Science Foundation (NSF) under Contract ANIR-ITR 0082916.

S. De was with the Department of Electrical Engineering, State University of New York at Buffalo, Buffalo, NY 14260 USA. He is now with the Department of Electrical and Computer Engineering, New Jersey Institute of Technology, Newark, NJ 07102 USA (e-mail: swades.k.de@njit.edu).

C. Qiao and S. J. Philip are with the Department of Computer Science and Engineering, State University of New York at Buffalo, Amherst, NY 14260 USA (e-mail: qiao@cse.buffalo.edu; sumeshjp@cse.buffalo.edu).

D. A. Pados is with the Department of Electrical Engineering, State University of New York at Buffalo, Amherst, NY 14260 USA (e-mail: pados@eng.buffalo.edu).

M. Chatterjee is with the Department of Electrical and Computer Engineering, University of Central Florida, Orlando, FL 32816 USA (email: mainak@cs.ucf.edu).

Digital Object Identifier 10.1109/JSAC.2004.829364

It is well-known that MAI is a key factor in determining the performance (e.g., throughput) of a code-division multiple-access (CDMA) network [7], [8]. Even if each node transmits at the lowest possible power to its intended receiver, lack of coordination (e.g., reservation [9] or request/acknowledgment [10] based transmission), and/or decentralized control mechanisms will result in a significant amount of interfering power from neighboring nodes. The interference problem becomes more severe as the node density increases, although at first sight a higher node density might otherwise help improve connectivity and network performance.

To avoid MAI altogether, Wieselthier *et al.* [11] considered an FH-CDMA-based system and proposed the use of small control packets to allocate frequency slots for data packets. Liu and Asada [12] proposed to contain MAI in a DS-CDMA-based sensor network through minimum energy channel coding and ON–OFF keying data transmission. In this approach, to deal with higher number of users, MAI is controlled by increasing the number of redundant bits (that is, lowering the channel code rate) at the cost of reduced information transmission rate. In [13], Dousse *et al.* assumed a time-division multiple-access (TDMA)-based channel access scheme on top of the CDMA codes to address the interference-related connectivity problem in a large ad hoc network. However, network (i.e., end-to-end routing) performance results were not presented. Muqattash and Krunz [14] proposed a controlled access CDMA protocol for wireless ad hoc networks, where out-of-band RTS-CTS (request-to-send/clear-to-send) packets were used to determine MAI before a data packet transmission and then the transmission power was adjusted accordingly. In terms of network connectivity, transmit power control-based connectivity maintenance in a random network setting was studied by Chen and Huang [15]. Kirousis *et al.* [16] provided a centralized algorithm for range allocation in a random network. Ramnathan and Rosales-Hain [17] studied topology control via centralized power allocation in static multihop networks and proposed heuristics to maintain connectivity in mobile multihop networks. Bettstetter [18] studied the relationship between k-connectivity and node density for a uniformly random node distribution, where a graph is said to be k-connected $(k \geq 1)$ if each node pair is connected via at least k mutually independent paths. Shakkottai *et al.* [19] studied network connectivity and coverage as a function of node coverage and failure probability under a grid topology, but did not take into account MAI and its impact on routing layer behavior. We note that, within the broad context of above-mentioned studies one also needs to consider the pertinent physical layer constraints. That way, for a given receiver structure and a corresponding acceptable

packet error performance, an optimum (in some sense) network topology can be determined (or, conversely, for a given network topology, a receiver design can be cost-optimized to achieve a target error performance).

In this paper, we first analytically characterize the MAI in a wireless CDMA network embedded in a plane with a random topology and study the associated tradeoff with k-connectivity. Instead of attempting to minimize MAI via controlled channel access (e.g., using ready-to-send–clear-to-send (RTS-CTS) or TDMA) or exclusively at the channel code design level, we propose to control MAI to a certain extent by proper placement/activation of nodes for a given signature code set and receiver structure, while maintaining the desired graph connectivity. To this end, we introduce a triangular topology. We study the link-level (i.e., single-hop) bit-error-rate (BER) performance of different network topologies, such as random, hexagonal, square grid, and triangular, using conventional matched-filter (MF), as well as MAI suppressive minimum mean-square-error (MMSE) receivers [20] under Gold [21] or other recently identified minimum total-squared-correlation (minTSC) code assignments [22]. Then, we study the network level performance (end-to-end throughput) of the various topologies under the two different receiver designs and signature code assignments. To the best of our knowledge, this is the first multilayer study that evaluates the tradeoff between MAI and k-connectivity and captures the effects of physical layer MAI, receiver structure, and signature codes on network performance.

The main observations from our study can be summarized as follows.

1) Network topology plays an important role in receiver design simplification and, hence, realizing low-cost sensors.
2) Although the triangular topology requires slightly higher number of nodes and has slightly worse link-level MAI behavior compared with the two other regular topologies (square grid and hexagonal), the triangular topology has superior overall end-to-end routing performance with graceful degradation in the presence of node failures. This finding alone implies that one cannot evaluate system performance-based only on link-level studies.
3) Beyond a certain node failure rate, the network performance of a deterministic fixed regular topology can be significantly inferior to that of a dense random topology. We note that in practice we may approximate and maintain a regular topology by appropriately activating certain nodes in a random topology. In this context, it is important to study the performance of regular topologies since they give bounds on the performance that practical sensor networks can achieve and offer guidelines to desirable node placement/activation strategies.

The rest of this paper is organized as follows. In Section II, we derive the interference power distribution at a receiver in a wireless CDMA sensor network, where the nodes are randomly distributed. In Section III, k-connectivity versus MAI tradeoff in a random topology network is discussed and three competitive regular topologies (hexagonal, square grid, and triangular) are introduced. Section IV contains the physical layer considerations on the system performance. Link-level and network performance results are presented in Section V. Finally, in Section VI, discussions on related work is presented and a few concluding remarks are drawn.

II. MAI in Sensor Networks With Randomly Distributed Nodes

We assume that each sensor node is assigned a unique binary signature code. We note that we do not necessarily consider signature codes with perfectly zero cross correlation (such as the Walsh–Hadamard code sets) because of 1) the restriction in the number of available orthogonal codes (less than or equal to the given multiple-of-four code length) and 2) the loss of orthogonality in practice due to physical layer asynchronicity and/or multipath signal propagation. In general, due to nonzero cross correlation between node signatures, we understand that there is an upper limit in the number of simultaneously active nodes in the vicinity of a receiver (i.e., within the interference range of a receiver) so that the received signal-to-interference-plus-noise ratio (SINR) stays above a minimum operational threshold. Because of the assumed random deployment of nodes, it is not possible to pursue a deterministic solution on the maximum allowable number of simultaneously active nodes for a given target SINR. Instead, we will obtain the statistical distribution of interference power from a neighbor to the receiver under consideration, from which the expected total interference at a receiver can be obtained for a given node density.

To obtain the interference power distribution, we use the following assumptions and definitions.

- All nodes have an omni-directional transmit and receive antenna of the same gain.
- The *receiving distance* r_R is defined as the maximum distance from which a receiving node can correctly recover a transmitted signal.
- The *interference distance* r_I is defined as the maximum distance from which a receiving node can sense a carrier. Typically, $r_I \approx 2r_R$ [23].
- With high probability, only one of the nodes within a certain minimum distance $r_0 \geq 1$ *unit* is active (i.e., participates in sensing and routing activities). When $r_0 \ll r_R$, we can safely assume that the spatial distribution of active nodes remains uniformly random.
- The signal power level at each receiver is controlled by the corresponding transmitter and is equal to the lowest possible operational threshold. Since the internodal distance varies randomly, the required transmit power is different for different transmitter-receiver pairs.

Fig. 1 shows node w as the receiver under consideration. Node u, while transmitting to node v, acts as an interferer to node w.

In the following, unless otherwise stated, a variable in bold denotes a random variable (RV) and a variable in italics denotes a realization (sample value).

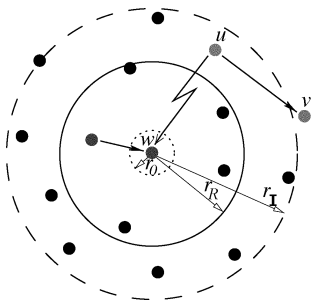

Fig. 1. MAI at node w from a local neighbor u.

A. Distribution of Interference Power

Let r denote the maximum radio frequency sensing range ($r_R \le r_I \le r$). If r_0 represents the minimum possible distance between any two active nodes, the cumulative distribution function (cdf) of the internodal distance $\mathbf{x}$ under uniformly random node deployment over a two-dimensional (2-D) space is given by

$$F_{\mathbf{x}}(x) = \begin{cases} \frac{x^2 - r_0^2}{r^2 - r_0^2}, & \text{in } (r_0, r] \\ 1, & x > r \\ 0, & x \le r_0 \end{cases}.$$

The corresponding probability density function (pdf) is

$$f_{\mathbf{x}}(x) = \begin{cases} \frac{2x}{r^2 - r_0^2}, & \text{in } (r_0, r] \\ 0, & \text{elsewhere} \end{cases}.$$

With the knowledge that signal power in wireless media decays proportionally to the distance raised to the power α, where the path loss parameter α varies between two and six, we define the RV $\mathbf{y} \triangleq \mathbf{x}^\alpha$. The cdf of $\mathbf{y}$ is

$$F_{\mathbf{y}}(y) = \begin{cases} F_{\mathbf{x}}\left(y^{\frac{1}{\alpha}}\right), & \text{in } (r_0^\alpha, r^\alpha] \\ 1, & y > r^\alpha \\ 0, & y \le r_0^\alpha \end{cases}.$$

From the above

$$f_{\mathbf{y}}(y) = \begin{cases} \frac{2y^{\frac{2}{\alpha}-1}}{\alpha\left(r^2 - r_0^2\right)}, & \text{in } (r_0^\alpha, r^\alpha] \\ 0, & \text{elsewhere} \end{cases}. \quad (1)$$

To determine the distribution of the transmit power from a node u to a local neighbor v, $\mathbf{p_{t,uv}}$, we note that to achieve a desired receive power threshold P_r,[1] the required transmit power $\mathbf{p_{t,uv}}$ increases with the distance d_{uv} raised to the power α (ignoring for the moment shadowing effects which will be considered later in Section IV)

$$\mathbf{p_{t,uv}} = P_r \mathbf{d}_{\mathbf{uv}}^\alpha, \quad r_0 < d_{uv} \le r_R. \quad (2)$$

[1]One could instead consider average output SINR threshold-based transmit power control, which is arguably much difficult to achieve in a random node placement setting with distributed power control. In this paper, we are interested in the interference from a randomly located interferer and we determine transmit power values based only on sender-destination distances.

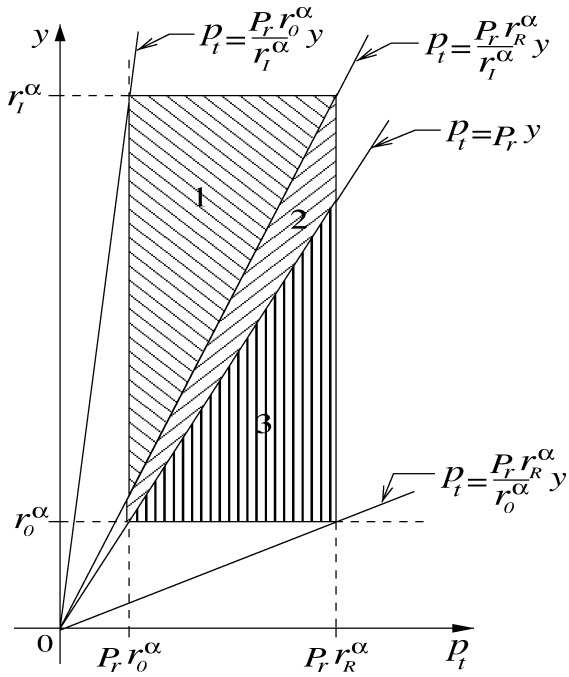

Fig. 2. Pictorial representation of the relation between $\mathbf{p_{t,uv}}$ and $\mathbf{d}_{\mathbf{uw}}^\alpha \triangleq \mathbf{y}$, where $p_t \sim (P_r r_m^\alpha, P_r r_R^\alpha]$, $y \sim (r_0^\alpha, r_I^\alpha]$.

P_r being constant, $\mathbf{p_{t,uv}}$ is an RV in $(P_r r_0^\alpha, P_r r_R^\alpha]$ with pdf

$$f_{\mathbf{p_{t,uv}}}(p_t) = \begin{cases} \frac{2p_t^{\frac{2}{\alpha}-1}}{\alpha P_r^{\frac{2}{\alpha}}\left(r_R^2 - r_0^2\right)}, & P_r r_0^\alpha < p_t \le P_r r_R^\alpha \\ 0, & \text{elsewhere} \end{cases}. \quad (3)$$

Referring to Fig. 1 for illustration purposes, the distance of the interfering transmitter u from the node of interest w, $\mathbf{d_{uw}}$, is an RV in $(r_0, r_I]$ and the interfering receive power at node w due to transmitter u is given by

$$\mathbf{p_I} = \frac{P_r \mathbf{d}_{\mathbf{uv}}^\alpha}{\mathbf{d}_{\mathbf{uw}}^\alpha}, \quad r_0 < d_{uv} \le r_R, \quad r_0 < d_{uw} \le r_I. \quad (4)$$

In Fig. 2, the horizontal axis represents the RV $\mathbf{p_{t,uv}}$ and the vertical axis represents the RV $\mathbf{d}_{\mathbf{uw}}^\alpha$. Three different regions (zones) can be identified as follows. Zone 1 corresponds to the case $(P_r r_0^\alpha)/(r_I^\alpha) < p_I < (P_r r_R^\alpha)/(r_I^\alpha)$, Zone 2 to the case $(P_r r_R^\alpha)/(r_I^\alpha) \le p_I < P_r$, and Zone 3 to the case $P_r \le p_I < (P_r r_R^\alpha)/(r_0^\alpha)$. With this breakdown, the cdf of $\mathbf{p_I}$ is obtained as follows.

Zone 1: $(P_r r_0^\alpha)/(r_I^\alpha) < p_I < (P_r r_R^\alpha)/(r_I^\alpha)$.

$$\begin{aligned} F_{\mathbf{p_I}}&\left(p_I \left| \frac{P_r r_0^\alpha}{r_I^\alpha} < p_I < \frac{P_r r_R^\alpha}{r_I^\alpha} \right.\right) \\ &= \int_{y=\frac{P_r r_0^\alpha}{p_I}}^{r_I^\alpha} \int_{p_t = P_r r_0^\alpha}^{y p_I} f_{\mathbf{p_{t,uv}}}(p_t) f_{\mathbf{y}}(y) dp_t dy \\ &= \frac{r_I^4 p_I^{\frac{2}{\alpha}} + P_r^{\frac{4}{\alpha}} r_0^4 p_I^{-\frac{2}{\alpha}} - 2P_r^{\frac{2}{\alpha}} r_0^2 r_I^2}{2P_r^{\frac{2}{\alpha}}\left(r_I^2 - r_0^2\right)\left(r_R^2 - r_0^2\right)}. \end{aligned} \quad (5)$$

Zone 2: $(P_r r_R^\alpha)/(r_I^\alpha) \le p_I < P_r$.

$$F_{\mathbf{p_I}}\left(p_I \left| \frac{P_r r_R^\alpha}{r_I^\alpha} \le p_I < P_r \right.\right) = \int_{y=\frac{r_0^\alpha r_I^\alpha}{r_R^\alpha}}^{r_I^\alpha} \int_{p_t=P_r r_0^\alpha}^{\frac{P_r r_R^\alpha}{r_I^\alpha} y} f_{\mathbf{p_t,uv}}(p_t) f_{\mathbf{y}}(y) dp_t dy + \int_{p_t=P_r r_0^\alpha}^{P_r r_R^\alpha} \int_{y=\frac{p_t}{p_I}}^{\frac{r_I^\alpha p_t}{P_r r_R^\alpha}} f_{\mathbf{p_t,uv}}(p_t) f_{\mathbf{y}}(y) dy dp_t = \frac{r_I^2}{(r_I^2 - r_0^2)} - \frac{(r_R^2 + r_0^2)}{2(r_I^2 - r_0^2)} P_r^{\frac{2}{\alpha}} p_I^{-\frac{2}{\alpha}}. \quad (6)$$

Zone 3: $P_r \le p_I < (P_r r_R^\alpha)/(r_0^\alpha)$.

$$F_{\mathbf{p_I}}\left(p_I \left| P_r \le p_I < \frac{P_r r_R^\alpha}{r_0^\alpha} \right.\right) = 1 - \int_{p_t=r_0^\alpha p_I}^{P_r r_R^\alpha} \int_{y=r_0^\alpha}^{\frac{p_t}{p_I}} f_{\mathbf{p_t,uv}}(p_t) f_{\mathbf{y}}(y) dy dp_t = 1 - \frac{r_0^4 p_I^{\frac{2}{\alpha}} + P_r^{\frac{4}{\alpha}} r_R^4 p_I^{-\frac{2}{\alpha}} - 2P_r^{\frac{2}{\alpha}} r_0^2 r_R^2}{2P_r^{\frac{2}{\alpha}} (r_I^2 - r_0^2)(r_R^2 - r_0^2)}. \quad (7)$$

Hence, from (5)–(7), the pdf of $\mathbf{p_I}$ is

$$f_{\mathbf{p_I}}(p_I) = \begin{cases} \frac{r_I^4 p_I^{\frac{2}{\alpha}-1} - P_r^{\frac{4}{\alpha}} r_0^4 p_I^{-\frac{2}{\alpha}-1}}{\alpha P_r^{\frac{2}{\alpha}} (r_I^2 - r_0^2)(r_R^2 - r_0^2)}, & \frac{P_r r_0^\alpha}{r_I^\alpha} < p_I < \frac{P_r r_R^\alpha}{r_I^\alpha} \\ \frac{P_r^{\frac{2}{\alpha}} (r_R^2 + r_0^2)}{\alpha (r_I^2 - r_0^2)} p_I^{-\frac{2}{\alpha}-1}, & \frac{P_r r_R^\alpha}{r_I^\alpha} \le p_I < P_r \\ \frac{P_r^{\frac{4}{\alpha}} r_R^4 p_I^{-\frac{2}{\alpha}-1} - r_0^4 p_I^{\frac{2}{\alpha}-1}}{\alpha P_r^{\frac{2}{\alpha}} (r_I^2 - r_0^2)(r_R^2 - r_0^2)}, & P_r \le p_I < \frac{P_r r_R^\alpha}{r_0^\alpha} \end{cases}. \quad (8)$$

An illustrative example to be followed throughout the rest of our presentation is given below.

Example: Consider $r_R = 25$ m, $r_I = 56$ m, $r_0 = 1$ m, $\alpha = 3.0$, and $P_r = -70$ dBm. The pdf of $\mathbf{p_I}$ as given in (8) is shown in Fig. 3. The Monte Carlo simulated pdf plot is obtained by randomly placing 2700 nodes in a 627.87×537.5 m^2 rectangular area. Simulation and analytic results match well. In the very low interference power region there is a certain lack of sufficient simulation data because the probability of having a given transmitter-receiver pair decreases with distance. □

Using our findings in (8), the mean value of the collected interference power η from an interfering node is given by

$$\eta = \frac{4P_r \left(r_R^{\alpha+2} - r_0^{\alpha+2}\right)\left(r_I^{\alpha-2} - r_0^{\alpha-2}\right)}{(\alpha^2 - 4) r_0^{\alpha-2} r_I^{\alpha-2} (r_I^2 - r_0^2)(r_R^2 - r_0^2)} \quad (9)$$

for $2 < \alpha \le 6$. Note that since in practice $\alpha > 2$, we do not consider the case $\alpha = 2$, which can be easily dealt with as a special case.

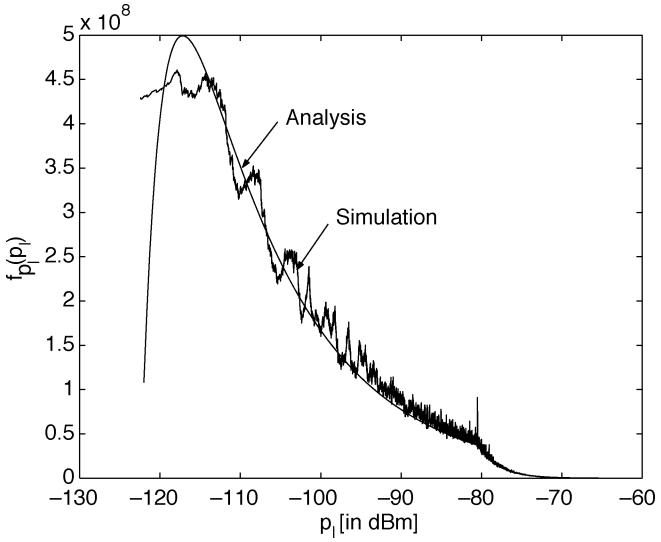

Fig. 3. Analytical [(8)] and simulated distribution of $\mathbf{p_I}$ ($r_0 = 1$ m, $r_R = 25$ m, $r_I = 56$ m, $\alpha = 3.0$, and $P_r = -70$ dBm).

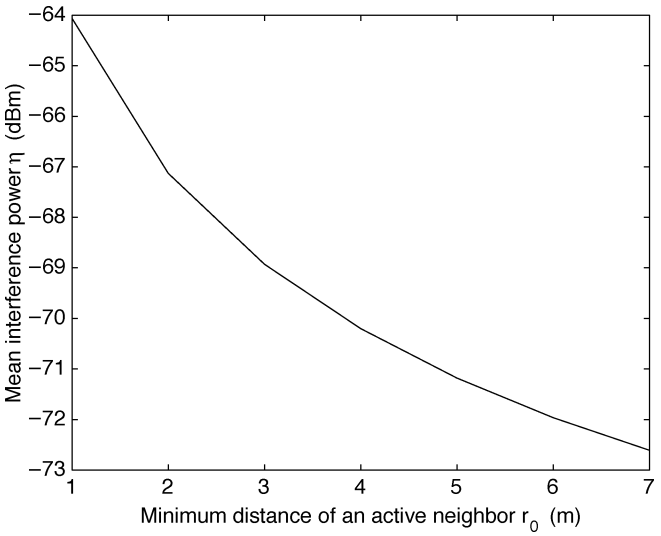

Fig. 4. Mean interference power from a neighboring transmitter [(9)]. As in Fig. 3, $r_R = 25$ m, $r_I = 56$ m, $\alpha = 3.0$, and $P_r = -70$ dBm.

Example (Continued): From (9), we obtain $\eta = -64.06$ dBm. Fig. 4 shows the impact of r_0 on the average interference power collected from a neighbor when r_0 varies from 1 to 7 m. We observe that decrease of r_0 increases the average interference power at a higher than linear rate. □

We now proceed to obtain an expression for the average number of *potential* interfering neighbors around a receiver.

B. Number of Potential Interfering Neighbors

The area covered by the interference range of a receiver (for example, node w in Fig. 1) is $a_I = \pi r_I^2$. If there are N nodes that are uniformly random distributed over a region of area A, the probability that a node has n neighbors within the interference range is binomially distributed

$$\Pr[n \text{ neighbors in the interference range}] = \binom{N-1}{n} \left(\frac{a_I}{A}\right)^n \left(1 - \frac{a_I}{A}\right)^{N-n-1}. \quad (10)$$

For $N \gg 1$ and $a_I \ll A$, the above binomial distribution is well approximated by the Poisson distribution

$$\Pr[n \text{ neighbors in the interference range}] \approx \frac{(\rho a_I)^n}{n!} e^{-\rho a_I} \tag{11}$$

where $\rho = N/A$ is the node density. Under the Poisson approximation, the expected number of nodes within the interference range of the receiver is

$$K = \sum_{n=0}^{N-1} n \frac{(\rho a_I)^n}{n!} e^{-\rho a_I} = \rho \pi r_I^2 \text{ for } N \gg 1 \text{ and } a_I \ll A. \tag{12}$$

Example (Continued): With $N = 2700$, $A = 627.87 \times 537.5$ m^2, and $r_I = 56$ m as before, we obtain a mean number of nodes within the interference range of a receiver $K = 79$. Note that only a fraction of the nodes within the interference range will be actual interferers and this fraction depends on a node's transmission activity and idling (i.e., failure or dormant state) probability. We do not attempt to calculate analytically the average number of actual interferers at this time. The actual interferers will be determined as necessary in simulation-based performance studies in Section IV. □

With this material in hand, we are now ready to examine the network k-connectivity issue.

III. Impact of Network Topology on k-Connectivity

Following Bettstetter [18], we note that degree-of-connectivity k implies that for all nodes in the network the minimum number of neighbors $k_{\min}$ is greater than or equal to k. For uniformly random distributed nodes, we can calculate

$$\Pr[k_{\min} \geq k] \equiv \Pr[\text{all nodes have at least } k \text{ neighbors in the reception range}] = \left(1 - \sum_{n=0}^{k-1} \frac{(\rho a_R)^n}{n!} e^{-\rho a_R}\right)^N \tag{13}$$

where $a_R = \pi r_R^2$.

It is well understood that all nodes having $k_{\min} \geq k$ does not ensure that the network (graph) is k-connected. There can be isolated islands of nodes (forming a multicomponent graph) with each node still satisfying $k_{\min} \geq k$. Thus

$$\Pr[k - \text{connectivity}] \leq \Pr[k_{\min} \geq k].$$

For asymptotically large networks ($N \to \infty$), Penrose [24] proved that

$$k - \text{connectivity} \underset{\text{in prob.}}{\overset{N \to \infty}{\longrightarrow}} k_{\min} \geq k, \tag{14}$$

i.e., $\Pr[k_{\min} \geq k]$ is a tight upper bound on the probability of k-connectivity of a network.

As we have stated in the introduction, we are interested in studying the tradeoff between connectivity (for successful routing) and MAI. We use the example introduced in the previous section as an illustration of the effect of MAI reduction on network connectivity for randomly distributed nodes.

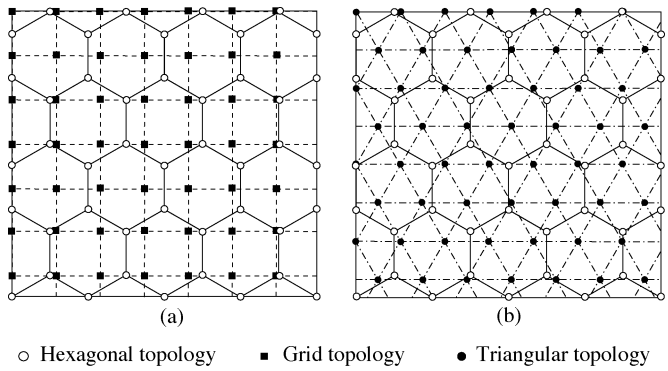

Fig. 5. Different regular network topologies with the same internodal distance (r_R). (a) Hexagonal and grid. (b) Hexagonal and triangular.

Example (Continued): Consider again $N = 2700$ and $A = 627.87 \times 537.5$ m^2, which gives $\rho = 0.008$. Using (11), with a_I replaced by $a_0 = \pi r_0^2$ and setting $r_0 = 1$ m, we obtain $\Pr[\text{no nodes within } r_0 \text{ range}] = e^{-\rho a_0} = 0.9752$. With $r_R = 25$ m, (13) gives $\Pr[k_{\min} \geq 1] = 0.9996$. Therefore, under this setting, the network satisfies one-connectivity (with probability close to 99.9%) and at the same time there is no active node around 1 m of the receiver (with probability 97.5%). To further reduce the interference power (cf., Fig. 4), we let $r_0 = 2$ m and keep $\Pr[\text{no nodes within } r_0 \text{ range}] = 0.9752$. To satisfy this probability, the required node density ρ becomes 0.002, or N becomes 675 for the given fixed deployment area A. If the receiving range r_R of a node is kept fixed at 25 m, from (13), we have $\Pr[k_{\min} \geq 1] = 1.47 \times 10^{-6}$. Hence, in attempting to reduce the interference, the nodes become practically isolated. □

The above example shows that if the active nodes remain uniformly random distributed, then it is not possible to maintain a desired high degree of network connectivity and have low MAI at the same time. In the context of MAI versus connectivity tradeoff, we suggest that for a given (high) node density at the time of deployment, low MAI and high connectivity can be achieved when the nodes are selectively activated such that *the set of active nodes at any time lies on the vertices of a regular polygon*. The regular polygon can be a square, or a hexagon, or an equilateral triangle, for example. As seen in Fig. 5, it is clear that with no node failures, the hexagonal topology offers three-connectivity, the square grid topology offers four-connectivity, and the triangular topology offers six-connectivity. We note that although we may not be able to achieve and perfectly maintain a regular topology in certain field applications, the performance of regular topologies (with no node failures) offers important bounds on the performance of practical sensor networks with distributed control.

To determine the number of nodes required in different regular topologies to cover an area A, we start with the hexagonal topology, where $N_{\text{hex}} = 2(M+1)^2$ nodes are placed over an $A = [((2M+1)\sqrt{3}r_R)/(2)] \times [((3M+1)r_R)/(2)]$ rectangular area for some integer M. In Fig. 5(a), for example, $M = 4$ and $N_{\text{hex}} = 50$. The number of active nodes required for the grid topology is $N_{\text{sqr}} = \lfloor(\sqrt{3}(2M+1))/(2)+1\rfloor\lfloor(3M+1)/(2)+1\rfloor$. The corresponding number for the triangular topology is $N_{\text{tri}} = \lfloor(\sqrt{3}(2M+1))/(2)+1\rfloor\lfloor(3M+1)/(2\sqrt{3})+1\rfloor+\lfloor(\sqrt{3}(2M+1)-1)/(2)+1\rfloor\lfloor((3M+1))-\sqrt{3})/(2\sqrt{3})+1\rfloor$. The number of nodes, N_{rnd}, required for the random topology

TABLE I
NUMBER OF NODES REQUIRED IN DIFFERENT TOPOLOGIES TO COVER A GIVEN LOCATION SPACE OF AREA $A = 627.87 \times 537.5$ m^2. ALL NODES HAVE EQUAL RECEPTION RANGE $r_R = 25$ m

Hexagonal (3-connected)	Square grid (4-connected)	Triangular (6-connected)	Random (1-connected with probability $\sim$0.9996)
450	572	638	2700

to fill in the same rectangular space, while ensuring 1-connectivity with high probability can be obtained from (13), where $\rho = (N_{\text{rnd}})/(A)$. Table I shows that the regular topologies achieve a significant gain with respect to the random topology in terms of number of nodes required to cover a given deployment area with a network of connectivity at least one.

To study the relative performance of the random and three regular topologies in Table I, we assume that the receiving range of a node r_R is equal to the arm length of a regular polygon (hexagon, grid, and triangle). The interference range is considered to be $r_I = \sqrt{5}r_R$. Within the $r_I = \sqrt{5}r_R$ range, the hexagonal topology has 12 nodes, the grid topology has 20 nodes, the triangular topology has 18 nodes, and the random topology has 79 nodes on average [see (12) and the related example].

In the sequel, we will study the MAI and end-to-end routing performance of the three regular topologies (hexagonal, grid, and triangular) and compare them with the random topology. For this purpose, we first need to establish the physical layer of our system.

IV. PHYSICAL LAYER CONSIDERATIONS

We adopt binary-phase-shift-keying (BPSK) CDMA modulation. The continuous-time received signal after carrier demodulation is modeled as [25, Chap. 5]

$$r(t) = \sum_{i} \sum_{k=1}^{K} \sqrt{E_k} b_k(i) s_k(t - iT) + n(t)$$

where E_k is the signal energy at the receiver under consideration from the kth transmitter within the interference range, $b_k(i) \in \{-1, +1\}$ is the ith transmitted information bit with duration T, and $s_k(t)$ is the transmitter signature (spreading code) of the form

$$s_k(t) = \sum_{j=1}^{L} c_k(j) P_{T_c}[t - (j-1)T_c]$$

where L is the system processing gain (signature length), $c_k(j) \in \{-1, +1\}$, $j = 1, \ldots, L$ are the assigned signature bits (or *chips*), for the kth transmitter, and $P_{T_c}(t)$ is the chip waveform (pulse) with duration $T_c = T/L$. For normalized signatures

$$\int_0^T s_k^2(t)dt = 1 \quad \forall k = 1, \ldots, K.$$

The received signal power due to node k is $10 \log_{10} E_k$ dB. The additive noise process $n(t)$ is assumed to be white Gaussian with power spectral density σ_{Th}^2.

The main attributes in a CDMA system that effect system cost and performance are: 1) signature codes and code length; 2) receiver design; and 3) CDMA signal synchronization. The relative performance of the four network topologies of interest is studied under the following system parameters.

1) **Signature Codes**: We consider *Gold sequences* [21] of chip length $L = 63$, which can support up to 65 users. In pursuit of low computational cost receiver operations, which can be achieved via using signature sequences of shorter length, we also consider *minimum total-squared-correlation (minTSC) codes* [22]. We consider, for example, chip length $L = 15$ that are available for any number of signatures/users up to $2^{L-1} = 2^{14}$. Note that minTSC codes are also optimum codes as Gold sequences, and unlike Gold codes, which can be of length $L = 2^m - 1$, $m \geq 4$, the length minTSC codes can vary widely (see [22], for more details). When using a minTSC code set of length 15 in a regular topology, the receiver signal setup remains mostly underloaded (i.e., the number of interfering neighbors K_I does not exceed 15). In contrast, in a random topology, the receivers are mostly overloaded (i.e., $15 < K_I$).
2) **CDMA Receiver**: First, we consider the conventional signature MF receiver, which is simple to realize but may be rather ineffective in the presence of moderate to severe MAI. Then, we consider active MAI suppression via MMSE filtering [20], which can be particularly important under overloaded signal conditions.
3) **Signal Synchronization**: Physical layer node/user CDMA signals can be either bit-synchronous or bit-asynchronous. We study both cases with the underlying assumption of chip-synchronicity.

Additionally, we study the system performance in the presence (or absence) of log-normal shadowing. The path loss parameter α is taken as 3.0. The log-normal path loss is calculated considering isotropic antennas of unity gain and operating frequency $f = 4$ GHz. Assuming that (for tiny sensors) the largest physical linear dimension of the antenna is $D \approx 1$ cm, we obtain the Fraunhofer distance [26, Chap. 3] $d_f = (2D^2)/(\lambda) \ll 1$ m, which verifies that the nodes outside $r_0 = 1$ m are indeed in the far field region, where the log-normal path loss equation is valid ($\lambda = c/f$ is the operating wavelength, where c is the speed of light in free space). The path loss up to $r_0 = 1$ m is obtained via the Friis free space equation [26, Chap. 3]. The standard deviation of the channel disturbance due to log-normal shadowing is considered to be $\sigma_{LN} = 8$ dB. A fading margin of 8 dB is set when log-normal shadowing is taken into account.

The desired receive power threshold is $P_r = -70$ dBm and the white Gaussian thermal noise power at the receiver is $\sigma_{Th}^2 = -80$ dBm. Hence, the desired signal-to-noise ratio (SNR) threshold is 10 dB. Unless otherwise stated, the transmission probability of a node is fixed at $p_{tx} = 0.5$.

V. PERFORMANCE RESULTS

In this section, we present link-level (i.e., one-hop) BER and network (i.e., end-to-end routing) performance results for the four topologies (random, hexagonal, grid, and triangular) under various system settings.

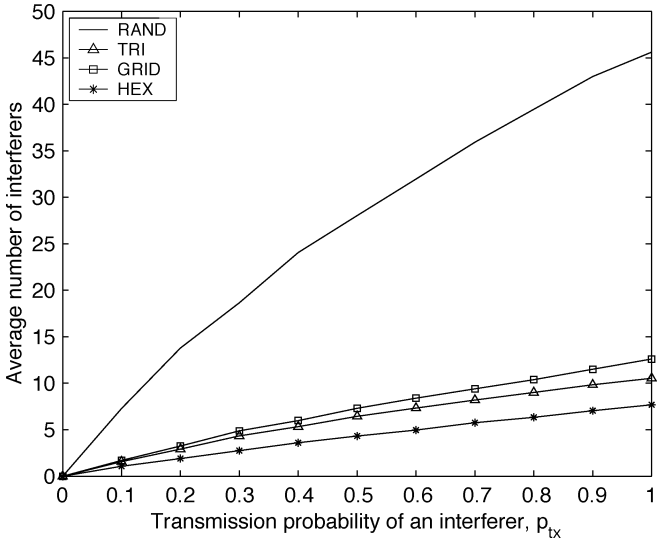

Fig. 6. Average number of interferers versus node transmission probability in different simulated network settings (idling/failure/sleeping node probability $p_f = 0$).

A. Link-Level Error Performance

When studying the link-level BER performance, we pick the receiver under consideration that is located well within the boundaries of the 627.87×537.5 m^2 field (i.e., at least $(r_I + r_R)$ m away from any boundary) to ensure that none of the potential interferers faces the border effect [18].

For the random topology, only one of the nodes within $r_0 = 1$ m is considered potentially active. For the regular topologies, there are certain deterministic interference signal power levels depending on the location of the interfering transmitters. For example, in the hexagonal topology there are at most *two* interferers with $\mathrm{SNR} = 10$ dB (at distance r_R), at most *six* interferers with $\mathrm{SNR} = 2.84$ dB (at distance $\sqrt{3}r_R$), and at most *three* interferers with $\mathrm{SNR} = 0.97$ dB (at distance $2r_R$).

Fig. 6 shows the average number of interferers as a function of the transmission probability p_{tx} for the four different topologies. When $p_{tx} = 1.0$, the maximum and minimum observed number of interferers in the random topology are 62 and 35, respectively. For the grid topology, these numbers are 16 and 12 and are maximum among the regular topologies when $r_I = \sqrt{5}r_R$. Therefore, when using the low-cost short minTSC code set, the receivers of a regular topology remain mostly underloaded, whereas in the random topology they are heavily overloaded.

Fig. 7 shows the relative performance of the three regular topologies, hexagonal, grid, and triangular, with MF receivers and $L = 63$ Gold codes. With *asynchronous signals* [Fig. 7(a) and (c)], the hexagonal topology performs the best irrespective of shadowing effects as its number of potential interferers is much fewer $(K = 12)$ compared with the triangular $(K = 18)$ and grid $(K = 20)$ topologies, respectively. We also note that even though the triangular topology has slightly fewer potential interferers, its MAI performance is somewhat inferior to the grid topology. This is because in the triangular topology, the interference SNR values at the receiver from farther away interferers are higher than the values for the grid (due to the specifics of the triangular node placement, cf., Fig. 5). For *synchronous systems*, performance differences are minimal and not worth mentioning. We do not present BER plots for MMSE receivers since under all circumstances (synchronous or asynchronous with or without shadowing) all three topologies have nearly indistinguishable performance.

With the understanding that among the three regular topologies the general link-level BER performance of the triangular topology is relatively the worst (although the difference is not very significant in most cases), we will compare the performance of the random topology to the triangular. In Fig. 8(a) and (c), we observe that with asynchronous MF receiver systems the random topology performs worse than the triangular with either short $(L = 15)$ minTSC or long $(L = 63)$ Gold codes. Usually, long Gold codes result in better BER (and more complex receiver). However, in the absence of shadowing effects, random topology with asynchronous, as well as synchronous receiver systems and long Gold codes performs even worse than the triangular topology with the short minTSC codes [cf., Fig. 8(a) and (b)]. In presence of shadowing [Fig. 8(c) and (d)], the triangular topology with minTSC codes performs slightly worse than the random topology with long Gold codes (specifically with asynchronous MF systems), indicating some sensitivity to channel conditions when short codes $(L = 15)$ are used. In synchronous MF systems with or without shadowing, the triangular topology with either Gold codes or minTSC codes performs almost the same as the random topology with Gold codes.

When considering the interference suppressing MMSE receiver (Fig. 9), we observe that the triangular topology with either short minTSC codes or long Gold codes performs practically the same as the random topology with long Gold codes with or without shadowing and with either synchronous or asynchronous receivers. However, the random topology performs worst with minTSC codes in all cases. In general, MMSE receivers (which are more complex) will result in much better performance than MF receivers.

From the above discussions, we observe that with a regular topology (such as triangular), short minTSC codes, which leads to low-cost sensors, may be used to achieve good performance, whereas with random topology, long Gold codes need to be used. With these observations in mind, we are now ready to study the end-to-end throughput performance of a network with different topologies (random, hexagonal, grid, triangular), codes ($L = 63$ Gold, $L = 15$ minTSC), and receiver structures (MF, MMSE).

B. Network Performance

To compare the end-to-end routing efficiency of the three regular topologies in the absence of node failures, we calculate the actual distances that are covered by an equal number of hops (i.e., while consuming equal transmit-receive energy). We observe that it is difficult to compare the efficiency along a general direction. Therefore, referring to Fig. 5, we consider routing along 12 equispaced directions that are 30° apart starting at 0° with respect to the horizontal axis.

- *Along* 0° *and* 180°: $2H$ hops in hexagonal topology cover $\sqrt{3}r_R H$ distance; H hops in both grid and triangular

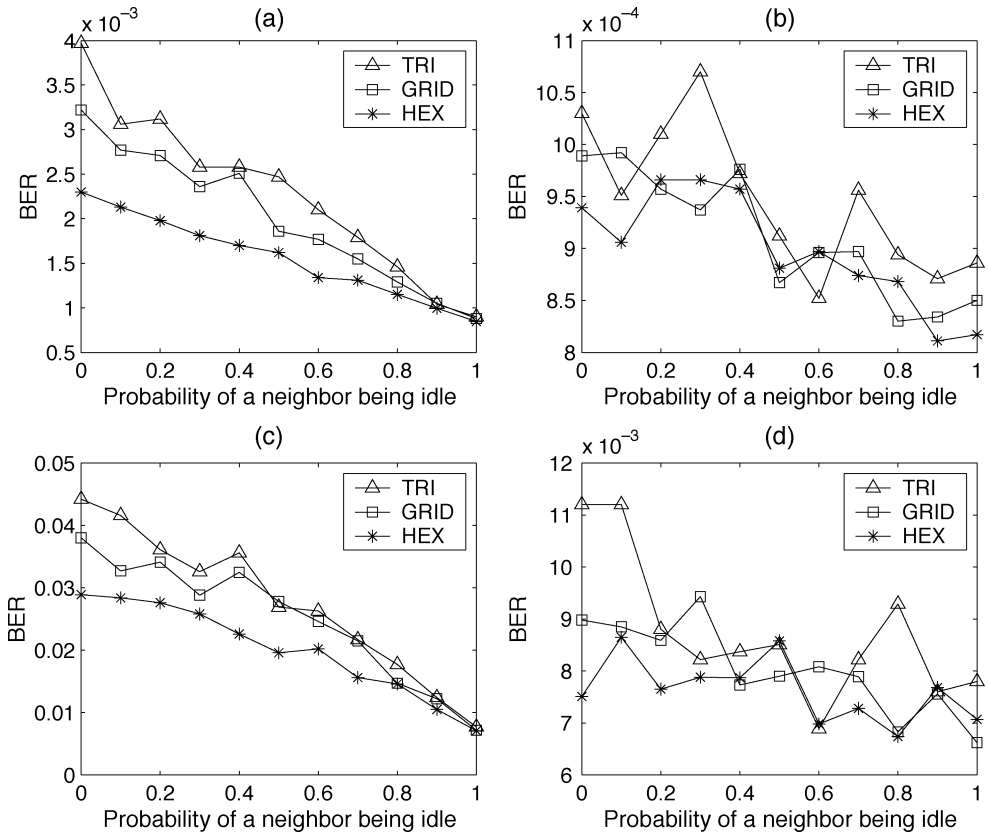

Fig. 7. Link-level BER performance of regular topologies with MF receiver and Gold codes ($L = 63$). (a) Async, no shadowing. (b) Sync, no shadowing. (c) Async, $\sigma_{LN} = 8$ dB. (d) Sync, $\sigma_{LN} = 8$ dB.

topology cover $r_R H$ distance. Thus, in an equal number of hops (i.e., $2H$) the ratio of distances covered in the hexagonal, grid, and triangular topology is $\sqrt{3} : 2 : 2$.

- *Along* 30°, 150°, 210°, *and* 330° (we note that for the grid topology the true angles are off by 0.06%): $4H$ hops in hexagonal topology cover $3r_R H$ distance; $41H$ hops in grid topology cover $\sqrt{901} r_R H$ distance; $2H$ hops in triangular topology cover $\sqrt{3} r_R H$ distance. So, in $164H$ hops the ratio of distances covered in the three topologies is $123 : 4\sqrt{901} : 82\sqrt{3}$.
- *Along* 60°, 120°, 240°, *and* 300° (for the grid topology the true angles are off by 0.06%): $2H$ hops in hexagonal topology cover $\sqrt{3} r_R H$ distance; $41H$ hops in grid topology cover $\sqrt{901} r_R H$ distance; H hops in triangular topology cover $r_R H$ distance. Therefore, in $82H$ hops the ratio of distances covered is $41\sqrt{3} : 2\sqrt{901} : 82$.
- *Along* 90° *and* 270°: $4H$ hops in hexagonal topology cover $3r_R H$ distance; H hops in grid topology cover $r_R H$ distance; $2H$ hops in triangular topology cover $\sqrt{3} r_R H$ distance. Therefore, in $4H$ hops the ratio of distances is $3 : 4 : 2\sqrt{3}$.

Considering all 12 cases above together, for an equal number of hops (i.e., $164H$) along any of these 12 specific directions, the ratio of actual distances covered in the hexagonal, grid, and triangular topology is 1:1.02:1.16. We recall (Table I) that the ratio of the number of nodes required to cover a given rectangular area in the three topologies is 1:1.27:1.42. Thus, while the grid topology requires quite a larger number of nodes to cover a given area, in the absence of node failures, the grid covers only a marginally longer distance than the hexagonal topology in equal number of hops. The triangular topology, with a relatively small number of extra nodes, covers a much larger distance.

To study the relative end-to-end routing performance via simulation, we consider the same 627.87×537.5 m^2 deployment area as in the link performance study, where 450, 572, 638, and 2700 nodes are placed in a hexagonal, grid, triangular, and random topology, respectively. The radio range of each node remains $r_R = 25$ m. The nodes are assumed to be location aware, and local broadcasts ensure that all nodes are also aware of their local neighbors' locations. For each topology, we simulate geographic forwarding at the network layer using GloMoSim [27]. Traffic sources and sinks are selected at random. Packets are forwarded using maximum forward with fixed radius (MFR) without backward progression [28], [29]. A packet is dropped if it cannot be forwarded further toward the final destination (due to lack of forwarding neighbors). Also, nodes have a fixed packet buffer of size 100 and packets are dropped without warning at an intermediate node if the buffer is full. There is no retransmission mechanism and data packets are considered lost when a receiver along the route is not able to decode packets due to high MAI. The radio transmission rate is 2 Mb/s. For each of the experiments described below, 20 random constaint bit rate CBR (CBR) sessions were initiated with each CBR source sending 5000 packets of size 50 Bytes to the destination. To obtain each point in the plots, five sets of data are taken. Our user-defined MAC layer only monitors the failure and sleep behavior of the local neighbors through an ideal common channel. For data packet transmission it emulates pure ALOHA protocol.

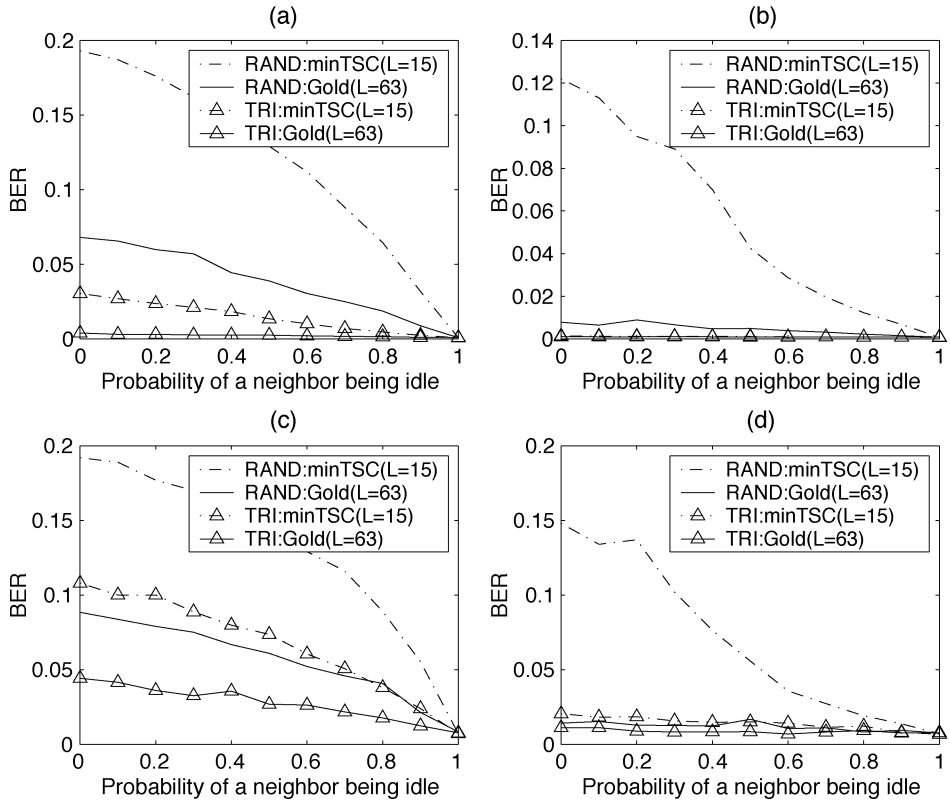

Fig. 8. Comparison of link-level BER performance of the random and triangular topology with MF receivers and long ($L = 63$) Gold or short ($L = 15$) minTSC codes. (a) Async, no shadowing. (b) Sync, no shadowing. (c) Async, $\sigma_{LN} = 8$ dB. (d) Sync, $\sigma_{LN} = 8$ dB.

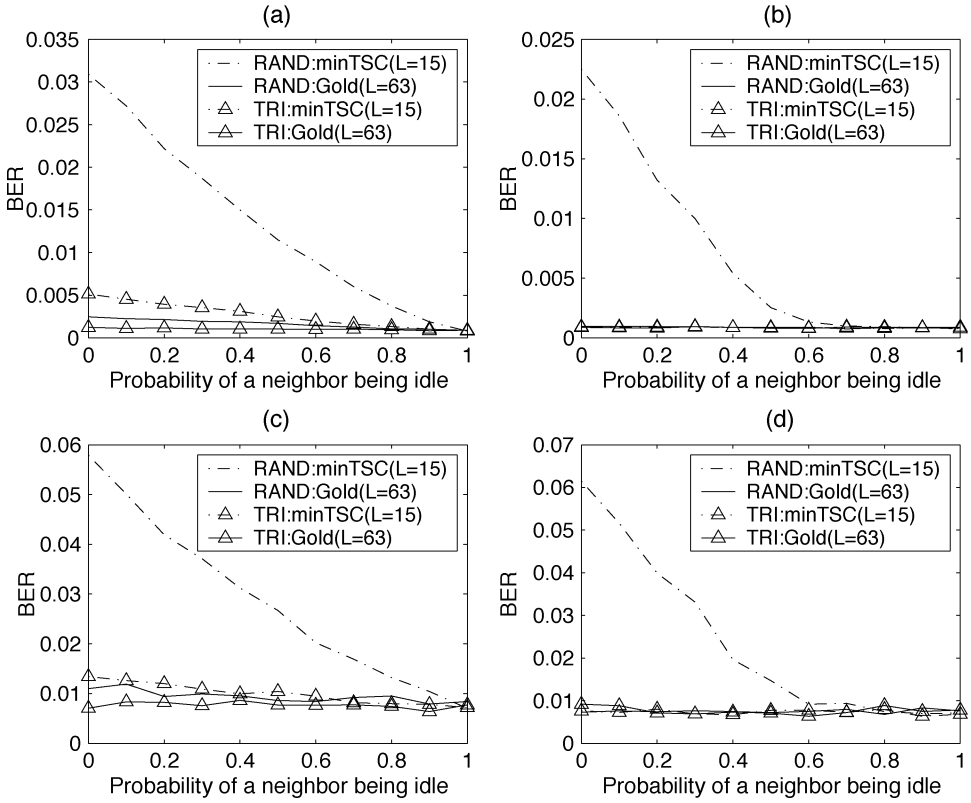

Fig. 9. Comparison of link-level BER performance of the random and triangular topology with MMSE receivers and long ($L = 63$) Gold or short ($L = 15$) minTSC codes. (a) Async, no shadowing. (b) Sync, no shadowing. (c) Async, $\sigma_{LN} = 8$ dB. (d) Sync, $\sigma_{LN} = 8$ dB.

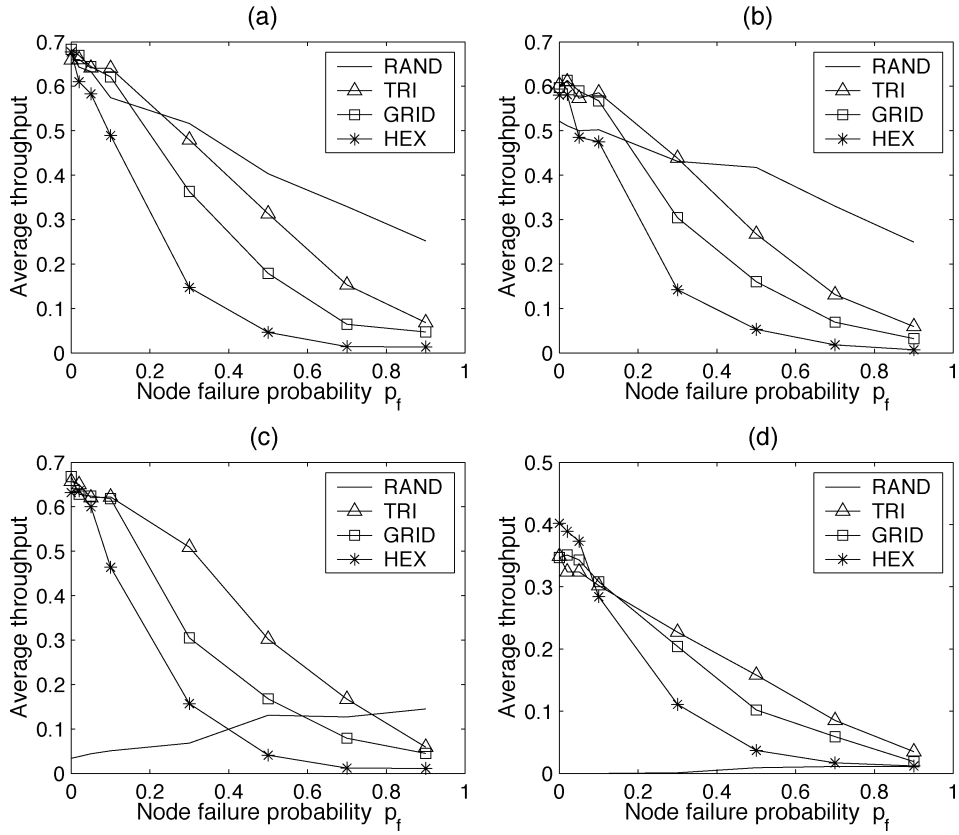

Fig. 10. Average throughput versus node failure probability in a synchronous system (failure recovery probability $p_r = 0.5$). (a) Gold $(L = 63)$, MMSE. (b) Gold $(L = 63)$, MF. (c) $\min\mathrm{TSC}(L = 15)$, MMSE. (d) $\min\mathrm{TSC}(L = 15)$, MF.

In the radio (physical) layer, we incorporate log-distance path loss and log-normal signal fading (shadowing), and implement the CDMA receiver of choice (MF or MMSE)—the parameters taken are the same as in our link-level simulations. In determining the MAI at the receivers along a route, it is assumed that all interfering users have different codes.

Since network connectivity is highly dependent on the status of nodes (failed/sleeping/active), it is important to study the exact effect of node failure and awake time on the network performance. To study intermittent node failure dependent network performance, we set the node sleeping probability p_s to zero, and in order to attain a steady state, we assume that when a node fails, either the node will recover or a neighbor will take over the routing task with probability p_r, called failure-recovery probability. Denoting the intermittent node failure probability by p_f and the *steady-state node failure probability* $p_{f-s}^{(f)}$, we have

$$\begin{aligned} p_{f-s}^{(f)} &= \Pr[\text{the node was OK}] \cdot \Pr[\text{failure}|\text{it was OK}] \\ &\quad \cdot \Pr[\text{recovery failed}] + \Pr[\text{the node was not OK}] \\ &\quad \cdot \Pr[\text{recovery failed}] \\ &= \left(1 - p_{f-s}^{(f)}\right) p_f (1 - p_r) + p_{f-s}^{(f)} (1 - p_r). \end{aligned}$$

Solving the above, we obtain

$$p_{f-s}^{(f)} = \frac{p_f (1 - p_r)}{1 - (1 - p_f)(1 - p_r)}. \tag{15}$$

Likewise, the effect of node sleep/awake time is captured by setting the intermittent node failure probability p_f to zero. The sleep time and awake time of a node are assumed to vary randomly between a preset minimum and maximum limit. Denoting the minimum and maximum sleep time and awake time by $T_{\mathrm{slp}}(\min)$, $T_{\mathrm{slp}}(\max)$, $T_{\mathrm{awk}}(\min)$, and $T_{\mathrm{awk}}(max)$, respectively, approximate *sleep-induced steady-state node failure probability* is

$$p_{f-s}^{(s)} = \frac{p_s \left(T_{\mathrm{slp}}(\max) - T_{\mathrm{slp}}(\min)\right)}{\left(T_{\mathrm{awk}}(\max) - T_{\mathrm{awk}}(\min)\right) + \left(T_{\mathrm{slp}}(\max) - T_{\mathrm{slp}}(\min)\right)}.$$

Based on the combined node failure probability $p_{f-s}^{(f)} + p_{f-s}^{(s)}$, a packet forwarding node is decided at the routing layer and the MAI-induced BER is obtained at the radio layer.

We first study intermittent node failure induced network throughput, where sleep probability p_s is assumed zero. Fig. 10 shows the throughput performance of a synchronous CDMA system with MF or MMSE receivers and long $(L = 63)$ Gold or short $(L = 15)$ minTSC code set. We observe that the performance of the regular topologies follows the same trend irrespective of receiver type and signature code set. In particular, the MAI performance of the short minTSC codes in a regular topology (i.e., an underloaded system) is as good as the long Gold codes, as also noted in link-level performance studies. Nevertheless, the performance of the hexagonal topology degrades sharply with an increase in the node failure probability because there are fewer nodes in this topology for route recovery. On the other hand, the decrease in throughput with node failure probability in the triangular topology is much slower

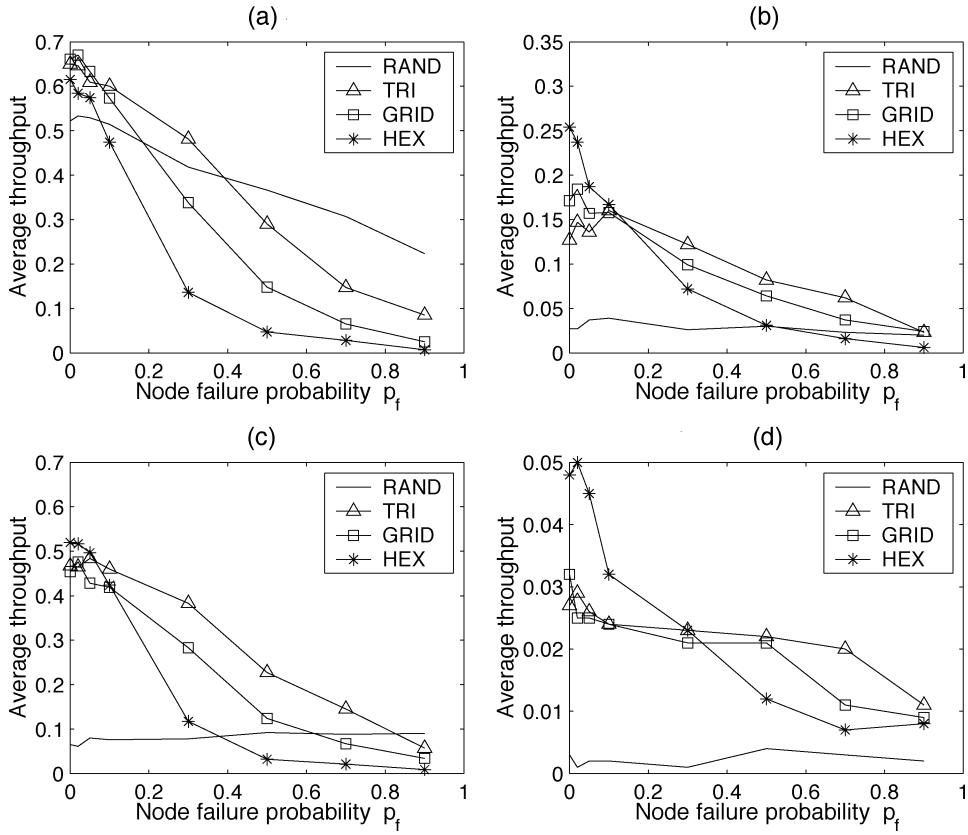

Fig. 11. Average throughput versus node failure probability in an asynchronous system (failure recovery probability $p_r = 0.5$). (a) Gold ($L = 63$), MMSE. (b) Gold ($L = 63$), MF. (c) $\min\mathrm{TSC}(L = 15)$, MMSE. (d) $\min\mathrm{TSC}(L = 15)$, MF.

than the other two regular topologies, indicating the highest resilience in a failure-prone node environment. As a result, the triangular topology has the best network performance (despite its worst link-level performance). Thus, *link-level performance alone may not give a complete picture and sometimes provides a misleading conclusion about the system performance*. We also note that in each of the regular topologies there is a "critical node failure probability" up to which the throughput performance is better than that in the random topology. This is because up to this critical probability, the chance of finding a route in a regular topology is still very high, whereas in the random topology MAI has not been reduced enough. With a further increase in failure probability, routing failure in the regular topologies overrides their advantages of having low MAI, resulting in lower throughput.

We further note from Fig. 10(a) and (b) that for the random topology with the long Gold codes, although the network has initially a lower throughput compared with the regular topologies (due to dominant MAI effects), its performance degrades at a much slower rate. Thus, at some (high) node failure probability, the throughput can be better than that of the regular topologies. When using the low-cost short minTSC codes in a dense random topology, the throughput is poor at low node failure probability [Fig. 10(c) and (d)] because of heavily overloaded receiver operation relative to the code length (which is consistent with the poor link-level performance of random topology with minTSC codes). The throughput increases with node failure probability due to reduction in MAI, which overrides the penalty of reduced connectivity.

The results with asynchronous users as shown in Fig. 11 are similar in trend to the synchronous case except that the MMSE receivers perform much better than MF receivers, and in addition, the random topology becomes less attractive even with long Gold codes since the benefits from reduced MAI cannot be obtained until we reach a higher node failure probability.

We note that in Figs. 10 and 11, the "effective" steady-state node failure probability [in (15)] does not increase beyond 0.5 even when p_f approaches 1.0. To capture the effect of a higher "effective" node failure probability, we can set $p_f = 1.0$ and vary p_r. Consider, as an example, a synchronous system with minTSC codes and with two different topologies—random and triangular. The dashed vertical lines in Fig. 12 show that with both MF and MMSE receivers the random topology system has two distinct performance regions (separated by dashed lines), the left of which is dominated by routing failure (i.e., k-connectivity), whereas the right side is dominated by MAI. Slightly right shifted vertical line corresponding to the MMSE receiver system indicates its more MAI resilience. The performance of triangular topology, on the other hand, is entirely dominated by routing failure.

Fig. 13 shows the average hop length of *successful* routes as a function of the node failure probability for all topologies with MF receivers and $L = 63$ Gold codes. While each of the regular topologies tries to recover from node failure via longer routes, beyond a certain failure probability only short routes can be found, which explains the results in this figure. Due to the substantially larger total number of nodes, the random topology is still able to recover via long routes.

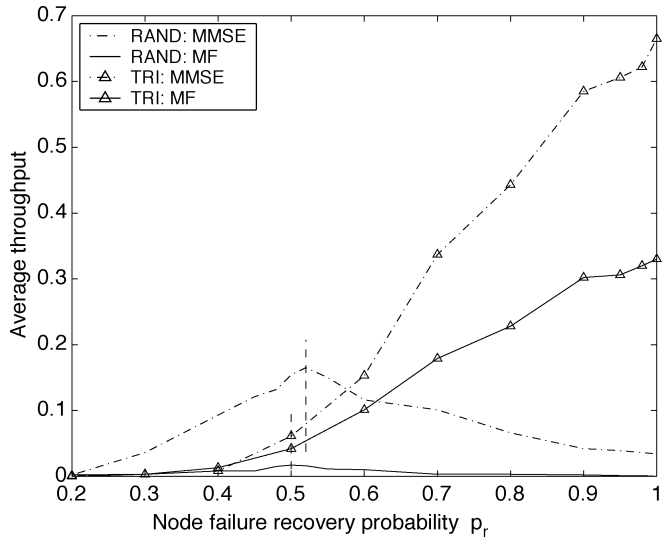

Fig. 12. Average throughput versus failure recovery probability in a synchronous system with random topology and minTSC codes $(L = 15)$ (intermittent node failure probability $p_f = 1.0$).

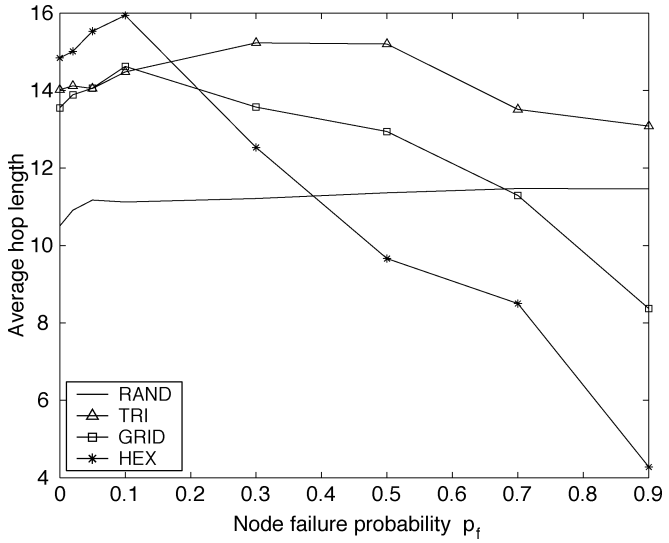

Fig. 13. Average hop length of successful routes versus node failure probability (synchronous system, Gold codes, MF receiver).

In Fig. 14, we examine the throughput performance as a function of the maximum node awake time $T_{\max}$. The actual awake time is modeled by a uniform RV that takes values between 1 and $T_{\max}$ s. Sleep time is also modeled as a uniform RV with values between 1 and 2 s. The sleep probability is set at 0.01 and the node failure probability p_f is zero. While the throughput of all regular topologies is relatively high and increases slightly with $T_{\max}$, for the random topology measurable throughput can be obtained only with the long $(L = 63)$ Gold codes. This is because with the chosen parameters the MAI for the random topology is too high under low-cost short $(L = 15)$ minTSC coding for both MF and MMSE receiver systems.

VI. Discussion and Conclusion

There has been a significant amount of work on cellular CDMA systems [7]. In such a scenario, to minimize the near–far effect, a base station controls the transmission power of the mobile nodes under its coverage. A mobile node, however, has no control over its surrounding interfering nodes and can only ask for higher power transmission from its base station. The interference at the nodes of a sensor network is similar to that at the mobile nodes in a CDMA network. However, the sensor network problem differs in terms of the limited processing power, energy constraints, low (or no) mobility of the sensor nodes, and the distributed control nature of the problem.

The use of spread-spectrum techniques (DS-SS and FH-SS) have been proposed in the 802.11 standard [10] and for Bluetooth systems [30]. The primary issue addressed in these systems is interference reduction in a heterogeneous environment rather than MAI control/reduction and its effects on the network performance. Chen and Boorstyn [31] analyzed the throughput of a multihop wireless CDMA system based on the assumption of equal noise effects from all interferers. However, such an assumption may not be appropriate in either random or regular network topologies. Chang and Tassiulas [32] studied the effect of power control for routing in multihop wireless networks to maximize network lifetime, but did not consider channel interference. Gupta and Kumar [33] analyzed the throughput capacity bounds for multihop wireless networks with a random topology. In their work, simultaneous transmission by multiple users was considered as pure noise, and receiver structure and signature code specific effects on the network performance were not captured.

There have also been some work on topology control. A clustering protocol for sensor networks called LEACH [34] utilizes a randomized rotation of a local cluster-head to distribute power consumption evenly among sensors. The SPAN protocol proposed by Chen *et al.* [35] provides an activity scheduling mechanism based on surrounding nodes' activity and network connectivity requirements. The SPAN approach attempts to form a hexagonal structure among the coordinator nodes to minimize the total number of nodes involved in routing (aiding to energy savings). Another energy conservation approach called geographic adaptive forwarding (GAF) proposed by Xu *et al.* [36] relies on location information. The entire geographic location is divided into virtual grids and, irrespective of the density of node deployment, one node remains active within each grid to maintain network connectivity. In a two-tier data dissemination model proposed by Ye *et al.* [37], each (randomly located) data generating node divides the network into a virtual grid with itself at the corner. Each node closest to the corner of a grid acts as a potential forwarding node. In this scheme, if there is a number of geographically distributed nodes generating data, then the forwarding nodes from each grid set (due to different data generating nodes) will form a set of randomly located active nodes.

We note that although there have been individual proposals and performance studies of grid and hexagonal topologies, to the best of our knowledge, comparative studies of the regular topologies and the random topology have not been reported. In this paper, specifically, we studied the physical layer constraints on link-level and network-level performance of a wireless CDMA sensor network. We characterized theoretically the MAI in

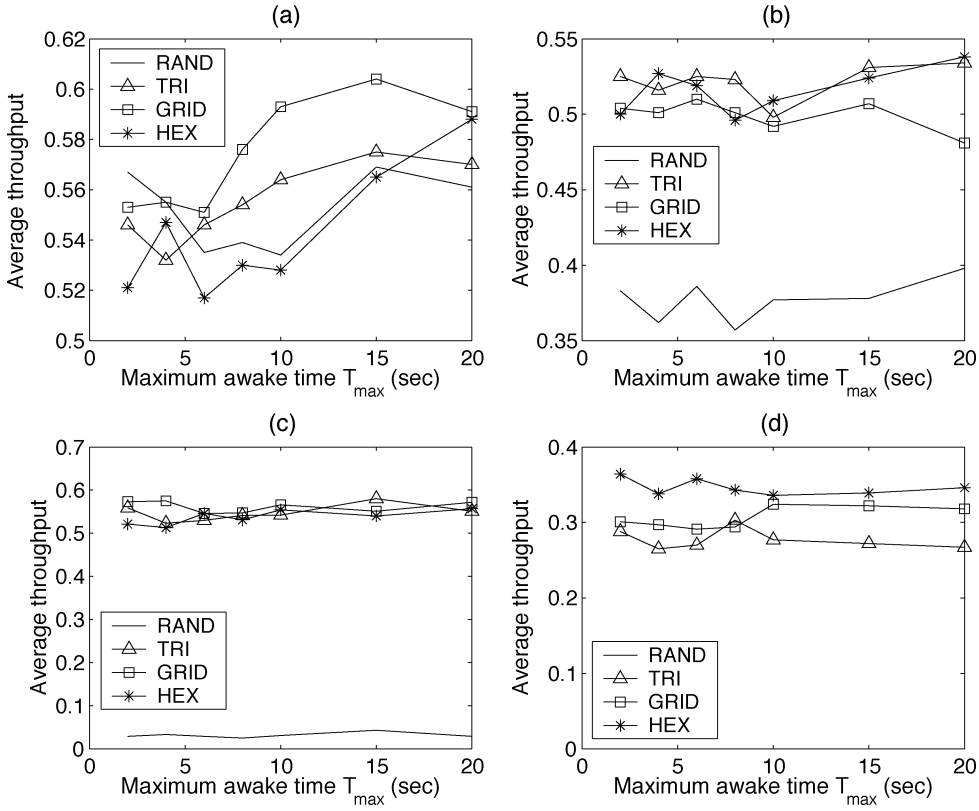

Fig. 14. Impact of node sleeping behavior on end-to-end routing performance. (a) Gold ($L = 63$), MMSE; (b) Gold ($L = 63$), MF. (c) $\mathrm{minTSC}(L = 15)$, MMSE. (d) $\mathrm{minTSC}(L = 15)$, MF.

a random topology network and showed that high network connectivity cannot be achieved without significantly increased MAI. To achieve a good MAI versus network connectivity tradeoff, we introduced a triangular topology. We studied the link-level (BER) and network-level (throughput) performance of the triangular topology, as well as the hexagonal, square grid, and random topology using conventional MF and MAI suppressive MMSE receivers with Gold signature code sets of length 63 and minTSC code sets of length 15.

The main conclusions from our performance evaluation are the following.

1) Network topology has a strong impact on potential receiver/signature design simplification (and hence, on sensor cost).
2) Although the triangular topology requires a slightly larger number of nodes and creates a somewhat stronger MAI environment than the other two regular topologies, its overall end-to-end routing performance is superior and has much more graceful degradation in failure-prone sensor networks.
3) It is beneficial to use a regular (for example, triangular) topology only up to a certain node failure rate beyond which throughput performance drops sharply well below the level of a corresponding (dense) random topology.

Our results can be useful as a performance benchmark study for different node activation/deployment strategies in field sensor networks, other radio receiver designs, and minTSC signature assignments of other lengths.

ACKNOWLEDGMENT

The authors are thankful to the anonymous reviewers for the useful comments in improving the presentation of the paper.

REFERENCES

[1] I. F. Akyildiz, W. Su, Y. Sankarasubramaniam, and E. Cayirci, "Wireless sensor networks: A survey," *Comput. Networks*, vol. 38, pp. 393–422, Mar. 2002.
[2] D. Estrin, R. Govindan, J. Heidemann, and S. Kumar, "Next century challenges: Scalable coordination in sensor networks," in *Proc. ACM MOBICOM*, Seattle, WA, Aug. 1999, pp. 263–270.
[3] N. Bulusu, J. Heidemann, and D. Estrin, "GPS-less low cost outdoor localization for very small devices," *IEEE Pers. Commun. Mag.*, pp. 28–34, Oct. 2000.
[4] C. Savarese, J. Rabaey, and J. Beutel, "Locating in distributed ad hoc wireless sensor networks," in *Proc. ICASSP*, Salt Lake City, UT, May 2001, pp. 2037–2040.
[5] A. Savvides, C. C. Han, and M. B. Srivastava, "Dynamic fine-grained localization in ad hoc networks of sensors," in *Proc. ACM MOBICOM*, Rome, Italy, July 2001, pp. 166–179.
[6] A. Nasipuri and K. Li, "A directionality based location discovery scheme for wireless sensor networks," in *Proc. ACM Workshop Wireless Sensor Networks Applications (WSNA)*, Atlanta, GA, Sept. 2002, pp. 105–111.
[7] A. J. Viterbi, *CDMA: Principles of Spread Spectrum Communications*. Reading, MA: Addison-Wesley, 1995.
[8] S. Gopalan, G. N. Karystinos, and D. A. Pados, "Capacity, throughput, and delay of slotted Aloha DS-CDMA links with adaptive space-time auxiliary-vector receivers," *IEEE Trans. Wireless Commun.*, to be published.
[9] D. J. Goodman, R. A. Valenzuela, K. T. Gayliard, and B. Ramamurthi, "Packet reservation multiple access for local wireless communications," *IEEE Trans. Commun.*, vol. 37, pp. 885–890, Aug. 1989.
[10] *Medium access control (MAC) and physical (PHY) specifications, Section 15*, ANSI/IEEE Standard 802.11, 1999.

[11] J. E. Wieselthier, A. Ephremides, and J. A. B. Tarr, "A distributed reservation-based CDMA protocol that does not require feedback information," *IEEE Trans. Commun.*, vol. 36, pp. 913–923, Aug. 1988.
[12] C.-H. Liu and H. H. Asada, "A source coding and modulation method for power saving and interference reduction in DS-CDMA sensor network systems," in *Proc. American Control Conf.*, Anchorage, AK, May 2002, pp. 3003–3008.
[13] O. Dousse, F. Baccelli, and P. Thiran, "Impact of interference on connectivity in ad hoc networks," in *Proc. IEEE INFOCOM*, San Francisco, CA, Apr. 2003, pp. 1724–1733.
[14] A. Muqattash and M. Krunz, "CDMA-based MAC protocol for wireless ad hoc networks," in *Proc. ACM MobiHoc*, Annapolis, MD, June 2003, pp. 153–164.
[15] W.-T. Chen and N.-F. Huang, "The strongly connecting problem on multihop packet radio networks," *IEEE Trans. Commun.*, vol. 37, pp. 293–295, Mar. 1989.
[16] L. M. Kirousis, E. Kranakis, D. Krizanc, and A. Pelc, "Power consumption in packet radio networks," *Theor. Comput. Sci.*, vol. 243, pp. 289–305, July 2000.
[17] R. Ramnathan and R. Rosales-Hain, "Topology control of multihop wireless networks using transmit power adjustment," in *Proc. IEEE INFOCOM*, Tel-Aviv, Israel, Mar. 2000, pp. 404–413.
[18] C. Bettstetter, "On the minimum node degree and connectivity of a wireless multihop network," in *Proc. ACM MobiHoc*, Lausanne, Switzerland, June 2002, pp. 80–91.
[19] S. Shakkottai, R. Srikant, and N. B. Shroff, "Unreliable sensor grids: Coverage, connectivity, and diameter," in *Proc. IEEE INFOCOM*, San Francisco, CA, Apr. 2003, pp. 1073–1083.
[20] M. L. Honig, U. Madhow, and S. Verdu, "Blind adaptive multiuser detection," *IEEE Trans. Inform. Theory*, vol. 41, pp. 944–960, July 1995.
[21] R. Gold, "Optimal binary sequences for spread spectrum multiplexing," *IEEE Trans. Inform. Theory*, vol. 8, pp. 619–621, Oct. 1967.
[22] G. N. Karystinos and D. A. Pados, "New bounds on the total squared correlation and optimum design of DS-CDMA binary signature sets," *IEEE Trans. Commun.*, vol. 51, pp. 48–51, Jan. 2003.
[23] A. Kamerman and L. Monteban, "WaveLAN-II: a high-performance wireless LAN for the unlicensed band," *Bell Labs Tech. J.*, vol. 2, pp. 118–133, Summer 1997.
[24] M. D. Penrose, "On k-connectivity for a geometric random graph," *Random Struct. Alg.*, vol. 15, pp. 145–164, 1999.
[25] S. Glisic and B. Vucetic, *Spread Spectrum CDMA Systems for Wireless Communications*. Norwood, MA: Artech House, 1997.
[26] T. Rappaport, *Wireless Communications: Principles and Practice*. Upper Saddle River, NJ: Prentice-Hall, 1996.
[27] X. Zeng, R. Bagrodia, and M. Gerla, "GloMoSim: A library for parallel simulation of large-scale wireless networks," in *Proc. 12th Workshop Parallel Distributed Systems (PADS)*, Banff, AB, Canada, May 1998, pp. 154–161.
[28] H. Takagi and L. Kleinrock, "Optimal transmission ranges for randomly distributed packet radio terminals," *IEEE Trans. Commun.*, vol. 32, pp. 246–257, Mar. 1984.
[29] T.-C. Hou and V. O. K. Li, "Transmission range control in multihop packet radio networks," *IEEE Trans. Commun.*, vol. 34, pp. 38–44, Jan. 1986.
[30] (2002, Nov.). [Online]. Available: http://www.bluetooth.org/specifications.htm
[31] M.-S. Chen and R. Boorstyn, "Throughput analysis of code division multiple access (CDMA) multihop packet radio networks in the presence of noise," in *Proc. IEEE INFOCOM*, Washington, DC, Mar. 1985, pp. 310–316.
[32] J.-H. Chang and L. Tassiulas, "Energy conserving routing in wireless ad hoc networks," in *Proc. IEEE INFOCOM*, Tel-Aviv, Israel, Mar. 2000, pp. 22–31.
[33] P. Gupta and P. R. Kumar, "The capacity of wireless networks," *IEEE Trans. Inform. Theory*, vol. 46, pp. 388–404, Mar. 2000.
[34] W. R. Heinzelman, W. R. Chandrakasan, and H. Balakrishnan, "Energy-efficient communication protocols for wireless microsensor networks," in *Proc. Hawaiian Int. Conf. Systems Science*, Maui, HI, Jan. 2000, pp. 3005–3014.
[35] B. Chen, K. Jamieson, H. Balakrishnan, and R. Morris, "Span: An energy-efficient coordination algorithm for topology maintenance in ad hoc wireless networks," in *Proc. ACM MOBICOM*, Rome, Italy, July 2001, pp. 85–96.
[36] Y. Xu, J. Heidemann, and D. Estrin, "Geography-informed energy conservation for ad hoc routing," in *Proc. ACM MOBICOM*, Rome, Italy, July 2001, pp. 70–84.
[37] F. Ye, H. Luo, J. Cheng, S. Lu, and L. Zhang, "A two-tier data dissemination model for large-scale wireless sensor networks," in *Proc. ACM MOBICOM*, Atlanta, GA, Sept. 2002, pp. 148–159.

Swades De (M'02) received the B.Tech. degree in radiophysics and electronics from the University of Calcutta, Calcutta, India, in 1993, the M.Tech. degree in optoelectronics and optical communication from Indian Institute of Technology, Delhi, in 1998, and the Ph.D. degree in electrical engineering from State University of New York at Buffalo, Amherst, in 2004.

From 1993 to 1997, he was a Hardware Development Engineer and during the first half of 1999, he was a Software Engineer with different telecommunication companies in India. During the first half of 2004, he was with the Istituto di Scienza e Technolozie dell' Informazione, National Research Council (ISTI-CNR), Pisa, Italy, through a European Research Fellowship. He is currently an Assistant Professor in the Department of Electrical and Computer Engineering, New Jersey Institute of Technology, Newark. His research interests include performance study, resource-efficient routing in multihop wireless networks and high-speed networks, integrated wireless technologies, and communication and systems issues in optical networks.

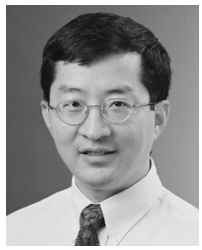

Chunming Qiao (S'89–M'93) directs the Laboratory for Advanced Network Design, Analysis, and Research (LANDER), State University of New York (SUNY) at Buffalo, Amherst, which conducts cutting-edge research work on optical networks, wireless networks, survivable networks, and TCP/IP technologies. He has published more than 120 papers in leading technical journals and conference proceedings. His pioneering research on optical Internet, in particular, the optical burst switching (OBS) paradigm is internationally acclaimed. In addition, his work on integrated cellular and ad hoc relaying systems (iCAR) is recognized as the harbinger for today's push toward the convergence between heterogeneous wireless technologies, and has been featured in *Businessweek* and *Wireless Europe*. He has given several keynotes, tutorials and invited talks on the above research topics.

Dr. Qiao is on the Editorial Board of several journals and magazines including the IEEE/ACM TRANSACTIONS ON NETWORKING and the *IEEE Communications Magazine*, and Guest Editor for several issues of the IEEE JOURNAL ON SELECTED AREAS IN COMMUNICATIONS (JSAC) and *ACM/Baltzer's Mobile Networks and Applications Journal* (MONET). He has chaired and cochaired 12 international conferences and workshops including the High-Speed Networking Workshop (formerly GBN) at INFOCOM 2001, INFOCOM 2002, OPTICOMM 2002, the Symposium on Optical Networks at ICC 2003, and the International Workshops on OBS (WOBS) at OPTICOMM 2003 and GLOBECOM 2003.

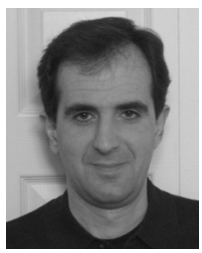

Dimitris A. Pados (M'95) was born in Athens, Greece, on October 22, 1966. He received the Diploma degree in computer science and engineering from the University of Patras, Patras, Greece, in 1989 and the Ph.D. degree in electrical engineering from the University of Virginia, Charlottesville, VA, in 1994.

From 1994 to 1997, he held an Assistant Professor position in the Department of Electrical and Computer Engineering and the Center for Telecommunications Studies, University of Louisiana, Lafayette. Since August 1997, he has been with the Department of Electrical Engineering, State University of New York at Buffalo, Amherst, where he is an Associate Professor. His research interests are in the general areas of communication theory and adaptive signal processing with emphasis on wireless multiple-access communications, spread-spectrum theory and applications, adaptive antenna arrays, and array radar.

Dr. Pados has been serving as an Associate Editor for the IEEE SIGNAL PROCESSING LETTERS and the IEEE TRANSACTIONS ON NEURAL NETWORKS since January 2000. Articles that he coauthored received the 2001 IEEE International Conference on Telecommunications Best Paper Award and the 2003 IEEE Transactions on Neural Networks Outstanding Paper Award.

Mainak Chatterjee received the B.Sc. degree in physics (Honors) from the University of Calcutta, Calcutta, India, in 1994, the M.E. degree in electrical communication engineering from the Indian Institute of Science, Bangalore, in 1998, and the Ph.D. degree from the Department of Computer Science and Engineering, University of Texas at Arlington, in 2002.

He is currently an Assistant Professor in the Department of Electrical and Computer Engineering, University of Central Florida, Orlando. His research interests include resource management and quality-of-service provisioning in wireless and cellular networks, sensor networks, CDMA data networking, media access control protocols, Internet traffic, and applied game theory.

Sumesh J. Philip received the B.Tech. degree in electronics and communication engineering from the National Institute of Technology, Calicut, India, in 1997 and the M.S. degree in computer science and engineering from the State University of New York (SUNY) at Buffalo, Amherst, in 2001. He is currently working toward the Ph.D degree in the Computer Science and Engineering Department, SUNY.

He has worked as a Summer Intern in Telcordia Technologies, Nokia Research, and Bell Laboratories, investigating issues related to wireless and cellular networks. His research interests include location and mobility management in mobile ad hoc and cellular networks, location tracking, and performance analysis of network protocols.